# Adaptive Compact Magnetic Tunnel Junction Model

Mohammad Kazemi, *Student Member, IEEE*, Engin Ipek, *Member, IEEE*, and Eby G. Friedman, *Fellow, IEEE*

***Abstract*— Electrical control of magnetic tunnel junctions (MTJs) provides opportunities to introduce MTJs into high-performance applications requiring low power consumption. The magnetic state of an MTJ can be electrically controlled through: 1) the spin transfer torque (STT) effect; 2) the voltage controlled magnetic anisotropy (VCMA) effect; and 3) the fusion of STT and VCMA. Several compact models have been published for MTJs. All of these models consider an MTJ whose magnetic state is controlled through the STT effect. In this paper, a model of an MTJ comprising a free layer, an analysis layer, and a spin polarizing layer is described. The MTJ compact model, adaptive compact MTJ (ACM) model, includes the effects of asymmetry on the MTJ behavior, and models a device controlled through the STT, VCMA, or a fused STT–VCMA mechanism. The ACM model includes the dynamics of the junction temperature. The proposed model can be adapted to experimental configurations including in-plane MTJ (IMTJ), IMTJ with a perpendicular-to-the-plane polarizer, perpendicular-to-the-plane MTJ (PMTJ), and PMTJ with an additional easy axis. The ACM model is validated with published experimental data, showing reasonably accurate results with an average error of less than 6%.**

***Index Terms*— Compact model, magnetic tunnel junction (MTJ), spin transfer torque (STT), voltage controlled magnetic anisotropy (VCMA).**

## I. Introduction

A MAGNETIC tunnel junction (MTJ) is a device whose electrical resistance is variable and depends on the magnetic state [1]. Electrically controlling the magnetic state of an MTJ offers opportunities to enhance the performance, density, functionality, and power consumption of a variety of applications ranging from memory [2]–[5] and logic [6] to RF oscillators [7]. The magnetic state of an MTJ can be electrically controlled through the spin transfer torque (STT) effect [8], the voltage controlled magnetic anisotropy (VCMA) effect [3], [9], or a combination of both the STT and VCMA effects [4].

The STT mechanism controls the magnetic state of an MTJ using current pulses that transport spin angular momentum. For a specific duration of the current pulse, the operation of the STT mechanism is maintained as long as the amplitude of the pulse is larger than a current threshold. Since the current threshold grows significantly as the duration of the pulse decreases, fast operation through the STT effect compromises the power efficiency and requires a high current density. Furthermore, the STT effect causes an MTJ to switch stochastically over a widely distributed switching time. This behavior is associated with the incubation time [10], which is the time for the system to absorb sufficient spin angular momentum from the injected spin polarized current to begin switching. The incubation time depends upon the thermal fluctuations of the magnetization, making the behavior of the MTJ stochastic. Recent experiments [10] show that incorporating a perpendicular polarizing layer into an MTJ removes the incubation time and enables deterministic, subnanosecond, and power efficient switching through the STT effect. High current densities are, however, required to switch the magnetic state of these MTJs.

The VCMA mechanism [3], [4], [9] has recently attracted considerable attention for spintronic applications operating at ultralow power levels. This mechanism controls the magnetic state of an MTJ through temporal change of the direction of the magnetic easy axis during application of a voltage pulse across the device. The VCMA mechanism offers a 500 times improvement in power efficiency as compared with the STT effect [9], and enables subnanosecond operation with no detectable incubation time. Reliable operation through the VCMA effect, however, requires precise subnanosecond control of the duration of the voltage pulse.

Both the STT and VCMA effects may coexist in an MTJ device [3], [4], and either of the effects can be of similar strength or dominate the other [3]–[5], [9]. Recent experiments propose hybrid switching mechanisms that employ both the STT and VCMA effects. A hybrid mechanism switches the magnetic state of an MTJ faster and more power efficiently than the STT mechanism and as reliably as the VCMA mechanism without requiring tight control of the duration of the voltage pulse applied across the device [3], [4].

An efficient compact model of an MTJ should accurately capture the device behavior in response to different controlling mechanisms of the magnetic state while maintaining high computational efficiency. Several compact models have been published for MTJs [11]–[19]. All of these models only consider an MTJ whose magnetic state is controlled through the STT effect. Furthermore, these models are accurate only for a symmetric MTJ, where both the free and analysis layers are composed of the same material. From both a device and circuit design point of view, a reliable compact model should accurately consider both the STT and VCMA effects, and be independent of device symmetry.

In this paper, a compact model, adaptive compact MTJ (ACM) model, is proposed. The ACM model considers both the STT and VCMA effects. The ACM model can

Manuscript received July 25, 2014; revised September 13, 2014; accepted September 16, 2014. Date of current version October 20, 2014. The review of this paper was arranged by Editor G. L. Snider.

M. Kazemi and E. G. Friedman are with the Department of Electrical and Computer Engineering, University of Rochester, Rochester, NY 14627 USA (e-mail: mkazemi@ece.rochester.edu; friedman@ece.rochester.edu).

E. Ipek is with the Department of Computer Science and the Department of Electrical and Computer Engineering, University of Rochester, Rochester, NY 14627 USA (e-mail: ipek@cs.rochester.edu).

Color versions of one or more of the figures in this paper are available online at http://ieeexplore.ieee.org.

Digital Object Identifier 10.1109/TED.2014.2359627

TABLE I
EXPERIMENTAL GEOMETRIES OF AN MTJ

| Geometry | $\theta$ | $\mathbf{H}_{kx}$ | $\mathbf{H}_{kz}$ | Polarizer orientation |
|---|---|---|---|---|
| IMTJ with perpendicular polarizer | 0 | Demagnetization field | In-plane anisotropy | $\mathbf{e}_x$ |
| IMTJ | 0 | Demagnetization field | In-plane anisotropy | No polarizer |
| PMTJ with additional in-plane easy axis | $\pi/2$ | In-plane anisotropy | Perpendicular anisotropy | No polarizer |
| PMTJ | $\pi/2$ | 0 | Perpendicular anisotropy | No polarizer |

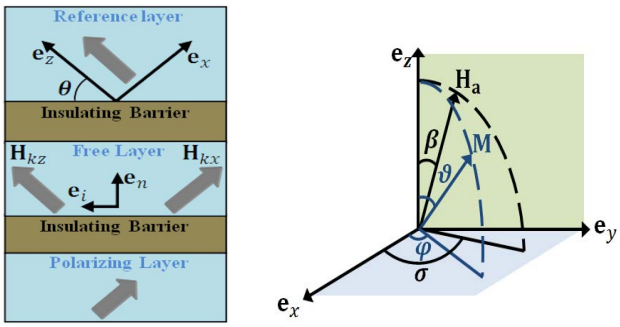


Fig. 1. Generalized structure of an MTJ. (a) Physical structure of the MTJ with two orthogonal magnetic anisotropies in the free layer. $\theta$ is the angle subtended by $\mathbf{e}_z$ and in-plane direction $\mathbf{e}_i$. The polarizing layer is magnetized perpendicular to the magnetization direction of the reference layer. (b) $\mathbf{H}_a$ is the applied magnetic field, and $\mathbf{M}$ is the magnetization of the free layer.

therefore be used to simulate an MTJ whose magnetic state is switched through either the STT mechanism or the VCMA mechanism as well as a hybrid STT-VCMA mechanism. The ACM model includes the effects of asymmetry on the physical behavior of the device. The ACM model can therefore be applied to either symmetric or asymmetric MTJs. The ACM model also includes the dynamics of the junction temperature (self-heating) and considers the effects of system temperature on the material properties. The ACM model can be adapted to any configuration including in-plane anisotropy MTJ (IMTJ), IMTJ with an additional polarizing layer, perpendicular-to-the-plane anisotropy MTJ (PMTJ), and PMTJ with an additional in-plane easy axis. The ACM model also provides the capability to simulate an MTJ under process variations.

The rest of this paper is organized as follows. The ACM model is characterized in Section II. Validation of the ACM model through experimental data is described in Section III. A comparison between the ACM model and previously proposed compact models is provided in Section IV. Finally, this paper is concluded in Section V.

## II. ACM MODEL CHARACTERIZATION

In this section, the ACM model is characterized. This model is based on the single domain approximation [23], where it is assumed that the magnetization is spatially uniform in ferromagnetic (FM) materials, behaving as a single macroscopic magnetic moment. The ACM model has been developed using Verilog-A, a standard behavioral description language [28].

### A. Generalized Structure of an MTJ

An MTJ based on a generalized structure, as shown in Fig. 1(a), is considered. This structure allows the ACM model to be applied to different geometries. This system is composed of two FM layers separated by a tunneling barrier and implanted on a polarizing layer whose magnetization is aligned along the $\mathbf{e}_x$ direction. Depending on whether the FM layers are composed of the same material, the MTJ is referred to, respectively, as either symmetric or asymmetric [20]. Magnetization of one FM layer, referred to as the reference layer (also known as the analysis layer), is pinned toward the $\mathbf{e}_z$ direction by virtue of being thicker or exchange coupled to an anti-FM layer. The other FM layer, referred to as the free layer (also known as the storage layer), has two orthogonal anisotropies: one along the $\mathbf{e}_x$ direction, denoted by $\mathbf{H}_{kx}$, and the other along the $\mathbf{e}_z$ direction, denoted by $\mathbf{H}_{kz}$. The magnetic anisotropies can be either axial or planar.

The unit vector along the magnetization of the free layer $\mathbf{M}$, as shown in Fig. 1(b), makes an angle $\vartheta$ with $\mathbf{e}_z$, while the plane of $\mathbf{M}$ and $\mathbf{e}_z$ makes an angle $\varphi$ with $\mathbf{e}_x$. An applied magnetic field $\mathbf{H}_a$, as shown in Fig. 1(b), makes an angle $\beta$ with $\mathbf{e}_z$, while the plane of $\mathbf{H}_a$ and $\mathbf{e}_z$ makes an angle $\sigma$ with $\mathbf{e}_x$. A spin polarized current passes through the free layer as long as a voltage $V$ is applied across the device. The self-induced magnetic field of the current is negligible as long as the lateral size of the free layer is small, where the spin-current effect is expected to become dominant over the current-induced magnetic field [23]. The in-plane direction (perpendicular-to-the-plane direction), $\mathbf{e}_i$ ($\mathbf{e}_n$), makes an angle $\theta$ ($\pi/2-\theta$) with $\mathbf{e}_z$.

### B. Experimental Geometry of an MTJ

By setting $\theta$ (the $\mathbf{e}_x$ and $\mathbf{e}_z$ axes of the coordinate system with respect to the plane of the layers), as well as the amplitude and sign of the anisotropies of the free layer, the structure shown in Fig. 1 can be applied to different geometries including the four experimentally relevant geometries listed in Table I. The first geometry is the IMTJ with a perpendicular polarizer. An example of this geometry is a nanopillar with an elliptic cross section implanted on a perpendicular polarizer [10]. The generalized structure is adapted to this case by setting $\theta = 0$, ensuring that the anisotropy components $\mathbf{H}_{kx}$ and $\mathbf{H}_{kz}$ are aligned, respectively, with the $\mathbf{e}_n$ and $\mathbf{e}_i$ directions, and the polarizer is aligned with the $\mathbf{e}_n$ direction. $\mathbf{H}_{kz}$ represents the in-plane anisotropy field of the free layer. $\mathbf{H}_{kx}$ is negative and represents the demagnetizing field of the free layer, but may also include a perpendicular-to-the-plane anisotropy as long as the perpendicular-to-the-plane anisotropy

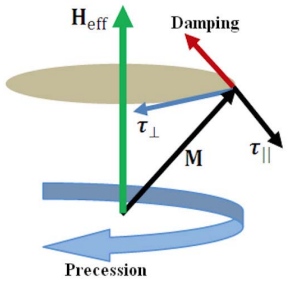


Fig. 2. Illustration of LLG dynamics. The magnetization $\mathbf{M}$ precesses around the effective magnetic field $\mathbf{H}_{\text{eff}}$.

does not overcome the demagnetizing field. For the remaining three geometries, the polarizing layer is removed. The second geometry is the IMTJ. The only difference between this case and the first case is the absence of a perpendicular polarizing layer.

The third geometry is the PMTJ with an additional in-plane easy axis. An example of this geometry is an elliptically shaped junction with perpendicular anisotropy. The generalized structure adapts to this geometry by ignoring the polarizing layer and setting $\theta = \pi/2$, ensuring that the anisotropies, $\mathbf{H}_{kx}$ and $\mathbf{H}_{kz}$, are aligned, respectively, with the $\mathbf{e}_i$ and $\mathbf{e}_n$ directions. Both of the magnetic anisotropies in this case are positive. The fourth geometry listed in Table I is the PMTJ. An example of this case is a nanopillar with a circular cross section [3]. The generalized structure is adapted to this geometry by removing the polarizing layer, and setting $\theta = \pi/2$ and $\mathbf{H}_{kx} = 0$, ensuring that the only intrinsic anisotropy is $\mathbf{H}_{kz}$, which is aligned with the $\mathbf{e}_n$ direction.

### C. Free Layer Magnetization Dynamics at Zero Temperature

The magnetization dynamics of the free layer is governed by the modified Landau–Lifshitz–Gilbert (LLG) equation,

$$\frac{d\mathbf{M}}{dt} = -\gamma\,\mathbf{M} \times \mathbf{H}_{\text{eff}} + \alpha\mathbf{M} \times \frac{d\mathbf{M}}{dt} - \gamma\,\boldsymbol{\tau}_{\text{STT}} \tag{1}$$

where $\mathbf{M}$ is the magnetization of the free layer, $t$ is the time variable, $\mathbf{H}_{\text{eff}}$ is the effective magnetic field experienced by the magnetization of the free layer, $\alpha$ is the Gilbert damping factor, $\gamma$ is the gyromagnetic ratio, and $\boldsymbol{\tau}_{\text{STT}}$ is the spin transfer torque. $\mathbf{H}_{\text{eff}}$ is derived from the magnetic anisotropy energies and the Zeeman energy as follows [23]:

$$\mathbf{H}_{\text{eff}} = -\nabla_{\mathbf{m}}\left[\frac{1}{2}\left(H_{ki}(\mathbf{m}\cdot\mathbf{e}_i)^2 + H_{kn}(V)(\mathbf{m}\cdot\mathbf{e}_n)^2\right) - \mathbf{m}\cdot(\mathbf{H}_a + \mathbf{H}_{\text{dipole}})\right] \tag{2}$$

where $\mathbf{m} = (\sin(\vartheta)\cos(\varphi), \sin(\vartheta)\sin(\varphi), \cos(\vartheta))$ is the unit vector parallel to $\mathbf{M}$, $H_{ki}$ is the amplitude of the in-plane anisotropy field, $H_{kn}(V)$ is the amplitude of the perpendicular-to-the-plane anisotropy field modulated by an applied voltage $V$ through the VCMA, $\mathbf{e}_i$ and $\mathbf{e}_n$ are, respectively, the unit vectors along the direction of the in-plane and perpendicular-to-the-plane of the MTJ, $\mathbf{H}_a$ is the externally applied magnetic field, and $\mathbf{H}_{\text{dipole}}$ is the sum of the magnetic fields exerted by the reference layer and polarizing layer.

As shown in Fig. 2, $\boldsymbol{\tau}_{\text{STT}}$ is composed of the in-plane torque ($\boldsymbol{\tau}_{\parallel}$) and the perpendicular torque ($\boldsymbol{\tau}_{\perp}$) normal to the $\boldsymbol{\tau}_{\parallel}$. Whereas $\boldsymbol{\tau}_{\perp}$ in fully metallic nanopillars is negligible [20], in MTJs, $\boldsymbol{\tau}_{\perp}$ can be as large as 30% of $\boldsymbol{\tau}_{\parallel}$ [21]. The choice of $\boldsymbol{\tau}_{\perp}$ must, therefore, be carefully considered in an MTJ model. Previous theoretical and experimental studies indicate that $\boldsymbol{\tau}_{\perp}$ is a symmetric function of the bias voltage $V$ [21], [22]. However, more recent studies show that the symmetric bias dependency is only accurate for symmetric MTJs, where both the free and reference layers are composed of the same material. In asymmetric MTJs, where the free and reference layers are made of different materials, $\boldsymbol{\tau}_{\perp}$ is an asymmetric function of the bias voltage [20]. Furthermore, unlike $\boldsymbol{\tau}_{\parallel}$, $\boldsymbol{\tau}_{\perp}$ is related to the exchange coupling energy between the magnetic layers and does not necessarily cancel when the voltage is set to zero [20]–[22]. Consequently, based on conservation of spin angular momentum, $\boldsymbol{\tau}_{\text{STT}}$ is

$$\begin{aligned}\boldsymbol{\tau}_{\text{STT}} &= \boldsymbol{\tau}_{\parallel} + \boldsymbol{\tau}_{\perp} \\ &= a_{\parallel} V \mathbf{M} \times ((\mathbf{M}_r + \zeta\mathbf{M}_p) \times \mathbf{M}) \\ &\quad + \left(\sum_{i=0}^{2} a_{\perp,\,i} V^i\right)(\mathbf{M}_r + \zeta\mathbf{M}_p) \times \mathbf{M}.\end{aligned} \tag{3}$$

Here, $\mathbf{M}_r$ and $\mathbf{M}_p$ are, respectively, the magnetization of the reference and polarizing layers, $\zeta \in [0, 1]$ determines the contribution of the polarizing layer to $\boldsymbol{\tau}_{\text{STT}}$, and prefactors $a_{\parallel}V$ and $\sum_{i=0}^{2} a_{\perp,i}V^i$ are, respectively, the bias dependent amplitude of the in-plane and perpendicular torques in the absence of a polarizing layer ($\zeta = 0$).

$\mathbf{M}_p$ and $\mathbf{M}$ are orthogonal for both parallel ($\mathbf{M}$ and $\mathbf{M}_r$ are parallel) and antiparallel ($\mathbf{M}$ and $\mathbf{M}_r$ are antiparallel) configurations. Therefore, independent of the configuration and polarity of the applied voltage (injected current) across (into) the device, the initial value of $\boldsymbol{\tau}_{\text{STT}}$ maintains a nonzero component against the damping torque ($\alpha\mathbf{M} \times (d\mathbf{M}/dt)$), which leads to precession of $\mathbf{M}$ and precessional switching. Note that $\boldsymbol{\tau}_{\text{STT}}$ also has a component which, depending on the polarity of the current pulse passing through the device and configuration, can either accelerate or dampen the switching process. Therefore, as reported experimentally in [10], both polarities are able to switch the IMTJ with a perpendicular polarizer, but with different switching probabilities.

$\mathbf{M}$ is constant in magnitude, suggesting that the coordinates $(\vartheta, \varphi)$ completely describe the temporal motion (precession and damping) of the free layer magnetization. The time derivative of $\vartheta$ and $\varphi$ appears independently in the LLG equation. Consequently, the LLG equation can be separated into two nonlinear first-order differential equations,

$$\frac{d\vartheta}{dt} = f_{\vartheta} + cf_{\varphi} \tag{4}$$

$$\sin(\vartheta)\frac{d\varphi}{dt} = cf_{\varphi} - f_{\vartheta}. \tag{5}$$

$c$ is a constant, and $f_{\vartheta}$ and $f_{\varphi}$ are nonlinear functions of $\vartheta$ and $\varphi$. As shown in Fig. 3, (4) and (5) characterize the behavior of a two-node capacitive circuit including two capacitors charged by dependent current sources. The current of each source is a function of the charge accumulated on both capacitors.

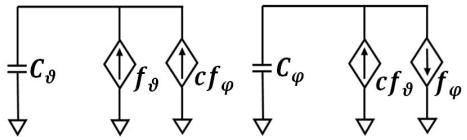


Fig. 3. Equivalent circuit of the LLG equation.

### *D. Free Layer Magnetization Dynamics at Finite Temperature*

A nonzero temperature causes the system to behave stochastically. Thermal effects can be included in the dynamic model through the addition of the Langevin random field $\mathbf{H}_L$ to the effective field. Each component of $\mathbf{H}_L$ is uncorrelated both in space and time and obeys a zero mean Gaussian distribution with variance $\delta^2 = 2\alpha k_B T/\mu_0\gamma M_s\Gamma$ [23]. Here, $\alpha$ is the magnetization damping factor, $\gamma$ is the gyromagnetic ratio, $\mu_0$ is the vacuum permeability, $k_B$ is the Boltzman constant, $M_s$ is the magnetization saturation, $\Gamma$ is the free layer volume, and $T$ is the system temperature, which is governed under the heat diffusion equation as follows:

$$\frac{\partial T}{\partial t} = \varepsilon\frac{\partial^2 T}{\partial x^2} + \frac{RA}{C_p\rho}J^2\delta(x). \tag{6}$$

$\varepsilon$ is the thermal diffusivity, $RA$ is the resistance area product of the junction, $C_p$ is the specific heat capacity, $\rho$ is the mass density of the material, and $J$ is the current density.

The heat diffusion equation is discretized in space for conversion into a system of ordinary differential equations,

$$\frac{d\mathbf{T}}{dt} = \mathbf{DT} + \frac{RA}{C_p\rho}J^2\mathbf{E} \tag{7}$$

where

$$\mathbf{T} = [T(x_1), \ldots, T(x_N)]^T$$

$$\mathbf{D} = \frac{\varepsilon}{(\Delta x)^2}\begin{bmatrix} -2 & 1 & 0 & 0 & \cdots & 0 \\ 1 & -2 & 1 & 0 & \cdots & 0 \\ \vdots & \ddots & \ddots & \ddots & \ddots & \vdots \\ 0 & \cdots & 0 & 1 & -2 & 1 \\ 0 & \cdots & 0 & 0 & 1 & -2 \end{bmatrix}$$

$$\mathbf{E} = [\delta(x_1), \ldots, \delta(x_N)]^T.$$

Equation (7) characterizes the behavior of a $(2N + 3)$-node distributed network of resistors ($R$) and capacitors ($C$) with an equivalent $RC$ $\pi$-circuit [27] as the basic component.

### *E. MTJ Conductance*

The conductance of an MTJ is the sum of two components: 1) an inelastic component that is a function of temperature and exhibits the spin-independent conductance of the device, and 2) an elastic component that is a function of the angle enclosed by the free and reference layers $\theta$, applied bias voltage $V$, and temperature $T$. This elastic component describes the spin-dependent conductance of the device.

The dependence of the elastic conductance on $\theta$ can be considered according to the tunneling magnetoresistance model presented in [1] and [24]. The voltage dependence of the elastic component at zero temperature is based on Brinkman's model [25]. The temperature dependence of both the elastic and inelastic conductances is considered according to Stratton's model [26]. Consequently, the tunneling conductance of the device is

$$\begin{aligned} G &= G_{\mathrm{SD}} + G_{\mathrm{SI}} \\ &= G_0\frac{\Lambda T}{\sin(\Lambda T)}\left[1 + P_1P_2\cos(\theta)\right]\sum_{i=0}^{2} C_i V^i + \mathrm{ST}^{1.33}. \end{aligned} \tag{8}$$

$G_0$ is the device tunneling conductance in a parallel configuration at zero temperature and zero bias, and defined as $G_0 \equiv (3.16 \times 10^{10}\ \tilde{\varphi}^{1/2}/d)\exp(-1.025 \times \tilde{\varphi}^{1/2}\ d)$, where $\tilde{\varphi}$ is the average tunneling barrier height, and $d$ is the tunneling barrier thickness. $\Lambda$ is a material and geometry-dependent parameter defined as $\Lambda \equiv 1.387\times10^{-4}\, d/\tilde{\varphi}^{1/2}$, $C_i$, $i \in \{0, 1, 2\}$, are material and geometry-dependent constants, as described in [25], $P_1$ and $P_2$ are, respectively, the temperature-dependent polarization factor of the free layer and reference layer, as described in [24], and $S$ is a fitting parameter, as described in [25].

### *F. Computational Complexity of the ACM Model*

As discussed in the previous two sections, the LLG and heat diffusion equations are, respectively, equivalent to a two-node capacitive and $(2\mathrm{N} + 3)$-node $RC$ network. Since the MTJ is a two-terminal device, the ACM model is equivalent to a $(2\mathrm{N} + 7)$-node $RC$ network. Parameter $N$ provides a tradeoff between accuracy and computational complexity. The ACM model is equipped with functions like bound_step [28] that provides a tradeoff between model accuracy and computational time. Nevertheless, the simulation engine that computes the ACM model affects the computational time. Cadence/Spectre [29], which is used for evaluating the model, provides three modes of operation—conservative, moderate, and liberal. Moving from the liberal toward the conservative mode of operation provides greater accuracy at the expense of increased computational time.

## III. Model Verification

The ACM model is shown to accurately match the experimental data, with an average error below 6%, for: 1) an asymmetric IMTJ switched through the STT mechanism [20]; 2) a symmetric IMTJ with a perpendicular polarizer (also known as a orthogonal spin torque MTJ device) [10] switched through the STT mechanism; and 3) a symmetric PMTJ switched through both the VCMA mechanism and a hybrid STT-VCMA mechanism [4].

### *A. Asymmetric IMTJ*

An asymmetric IMTJ (the second geometry listed in Table I) is considered. The ACM model variables are set according to the experimental data published in [20]. The lateral size of the device is $180 \times 80$ nm$^2$. The thickness of the free layer, tunneling barrier, and fixed layer is, respectively, 1.8, 0.7, and 2 nm. In this experiment, the VCMA effect is negligible and the magnetic state is controlled through

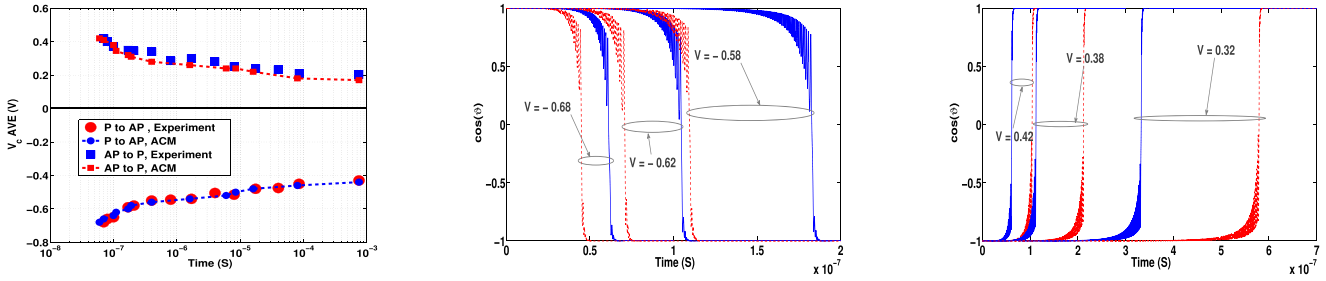


(a) (b) (c)

Fig. 4. Asymmetric MTJ switched through the STT effect. (a) Voltage versus log-scale pulse width at $T = 300$ K. (b) Transient switching from parallel configuration to antiparallel configuration. (c) Transient switching from antiparallel configuration to parallel configuration. In Fig. 4(b) and (c), the solid curves show the results determined from the ACM model, and the dashed curves show the results under the $\tau_\perp = 0$ approximation.

the STT effect. A voltage pulse applied across the device controls the amplitude of the current pulse that passes through the device. The average switching voltage versus the switching time is shown in Fig. 4(a). The ACM model accurately matches the experimental data from [20], exhibiting sufficient accuracy to capture the behavior of an asymmetric MTJ with a maximum error of 17.7% and a mean error of 5.7%.

The dashed curve in each clustered pair shown in Fig. 4(b) and (c) illustrates magnetization switching under the approximation $\tau_\perp = 0$, an approximation commonly used in previously published compact MTJ models [11]–[19]. As discussed in the previous section, this assumption is only valid when the device is symmetric. The solid curve in each selected pair shows magnetization switching based on the ACM model. Note that the error introduced by the $\tau_\perp = 0$ approximation increases significantly as the applied voltage decreases. This error is associated with the range of the applied voltage. As the applied voltage decreases within this range, $\tau_\perp$ becomes comparable with $\tau_\parallel$. The $\tau_\perp = 0$ approximation, therefore, introduces significant error.

Spin polarized current transfers spin angular momentum into the magnetic body of an MTJ, leading to spin transfer torque. The STT effect switches an MTJ (without a perpendicular polarizing layer) by magnifying the random variations of the free layer magnetization **M**. At higher temperatures, **M** experiences greater random variations. To switch the device, therefore, a smaller voltage and magnetic field needs to be applied to the device. Alternatively, at a specific ambient temperature, by increasing the amplitude of the voltage pulse applied to the device, more current passes through the device, increasing the junction temperature. **M**, therefore, experiences larger random variations, the initial value of $\tau_{\mathrm{STT}}$ becomes larger, and a smaller external magnetic field is required to switch the device. To illustrate the effects of temperature and self-heating on the device behavior, the switching phase diagram of an asymmetric IMTJ is evaluated for two different temperatures, 300 and 4.2 K. The ACM model variables are set according to the experimental data published in [20]. As observed in Fig. 5, the switching phase diagrams obtained through the ACM model follow the experimental data from [20], exhibiting sufficient accuracy to capture the effects of temperature and self-heating on the behavior of an MTJ with a maximum error of 19.2% and a mean error of 5.3%.

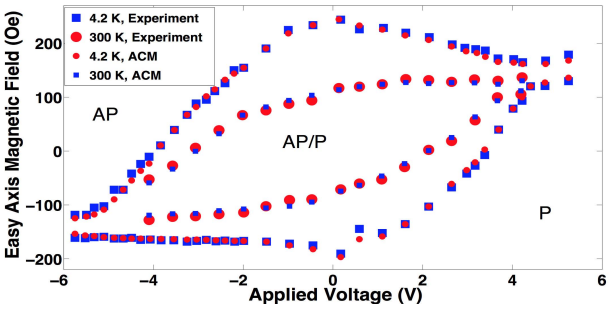


Fig. 5. Switching phase diagram at $T = 4.2$ K and $T = 300$ K. Experimental switching phase diagrams for an asymmetric IMTJ [20] is compared with the switching phase diagrams obtained through the ACM model.

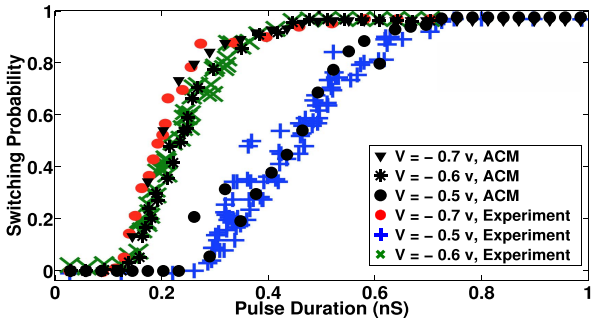


Fig. 6. Probability of switching from the parallel configuration to the antiparallel configuration as a function of pulse duration for three different pulse amplitudes. Experimental data [10] is compared with the data obtained through the ACM model.

### *B. Symmetric IMTJ With Perpendicular Polarizer*

Consider an IMTJ with a perpendicular polarizer [10]. The lateral size of the device is $180 \times 60$ nm$^2$. The thickness of the free layer, tunneling barrier, and fixed layer is, respectively, 3, 0.8, and 2.3 nm. In this experiment, the VCMA effect is negligible and the system is controlled through the STT effect. The voltage pulse applied across the device controls the amplitude of the current pulse that passes through the device. The switching probability from the parallel configuration to the antiparallel configuration is determined for voltage pulses with different amplitudes, 0.5, 0.6, and 0.7 V, and different durations up to 1 ns. The results generated by the ACM model are compared with the experimental results from [10] in Fig. 6.

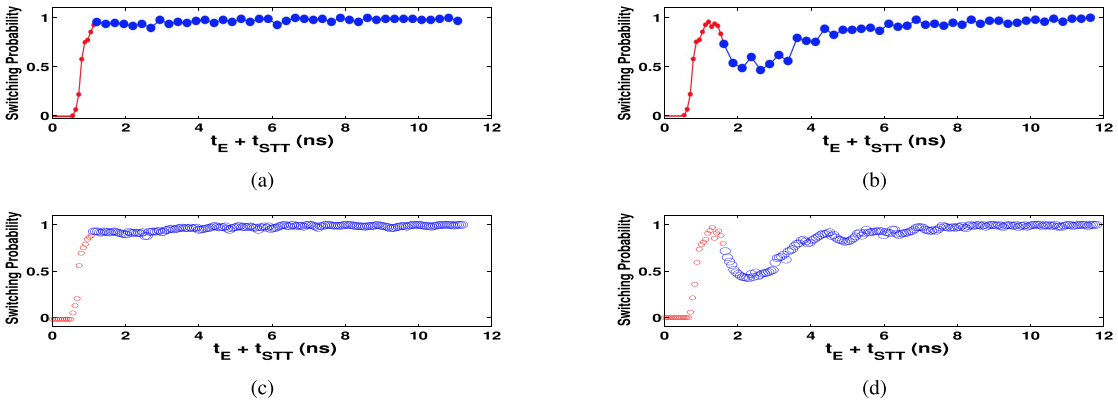


Fig. 7. Switching probability as a function of total pulse duration ($t_E + t_{STT}$) for parallel to antiparallel switching for different pulse durations. Figures 7(a) and 7(b) illustrate the experimental data. Figures 7(c) and 7(d) illustrate the data from the ACM model for the same parameters as, respectively, Figures 7(a) and 7(b). For all cases, $V_E = 0.7$ volts, and $V_{STT} = 0.5$ volts. Experimental data [4] is compared to the data obtained through the ACM model.

Note that the ACM model accurately follows the experimental data with a mean error of 4%.

Higher amplitude pulses lead to switching at shorter pulse durations. From both the experimental data and the ACM model, voltage pulses of 0.7 V amplitude and wider than 500 ps achieve a switching probability of 1. Consequently, there is no incubation delay of several nanoseconds as observed in previous experiments on MTJs without a polarizing layer.

### C. Hybrid STT-VCMA Mechanism

The hybrid STT-VCMA mechanism is considered, where the magnetic state of an MTJ is switched exploiting both the STT and VCMA effects. This hybrid mechanism switches the magnetization of a PMTJ through two consecutive voltage pulses applied across the device. The first pulse, with a relatively higher amplitude and a much shorter duration, initializes the magnetization precession though the VCMA effect. During application of the first pulse, the STT effect is much weaker and is negligible [4]. The second voltage pulse, of smaller amplitude but longer duration, stabilizes the magnetization switching direction through the STT effect assisted by the VCMA effect [4]. For a specific pulse duration, the amplitude of the first voltage pulse must be sufficiently high to exert a sufficiently strong initial torque to the device magnetization through the VCMA effect. Furthermore, for a specific pulse amplitude, the duration of the second pulse must be sufficiently long to apply sufficient STT to the precessing magnetization, thereby stabilizing the switching direction.

The parameters used in the ACM model are based on the experimental parameters from [4]. The device is of circular cross section with a diameter of 40 nm. The thickness of the free layer, tunneling barrier, and fixed layer is, respectively, 0.9, 1.3, and 1.8 nm. The first pulse has an amplitude of $V_E = 0.7$ V and a duration of $t_E$ to induce precessional motion of magnetization in the free layer through the VCMA effect. The second pulse has an amplitude of $V_{STT} = 0.5$ V and a duration of $t_{STT}$ to stabilize the resulting switching direction through the STT effect.

The probability of switching from the parallel state to the antiparallel state as a function of $t_E + t_{STT}$ is shown in Fig. 7. The experimental switching probabilities [4] are shown in Fig. 7(a) and (b). The switching probabilities determined from the ACM model for the same parameters used in Fig. 7(a) and (b) are shown, respectively, in Fig. 7(c) and (d). In all four figures, the small circles illustrate the switching probability when only the first voltage pulse is applied (VCMA mechanism), and the large circles depict the switching probability when both voltage pulses are applied (hybrid VCMA-STT mechanism). The results show that the ACM model accurately follows the experimental data with a maximum error of 22.1% and a mean error of 5.1%.

Note from Fig. 7 that when only the first pulse is applied (small circles), changing the pulse duration from 1.3 [Fig. 7(a) and (c)] to 1.7 ns [Fig. 7(b) and (d)] reduces the switching probability from 1 to 0.76. Hence, reliable switching through the VCMA mechanism requires the duration of the applied voltage pulse to be tightly controlled. Alternatively, the second applied pulse stabilizes the switching direction and maintains a high switching probability for a wide range of pulse durations without the need for tight control of the duration of the applied voltage pulses.

### D. Hybrid MTJ-CMOS Simulation with the ACM Model

To illustrate the capability of integrating the ACM model with CMOS for circuit level simulation, the operation of two relatively complex circuits is evaluated in this section: 1) an STT-Magnetoresistive Random Access Memory (MRAM) cell, and 2) a magnetic flip-flop (MFF). The resistance of an MTJ can take on two different stable values, $R_L$ and $R_H$. An MTJ, therefore, may store one bit of information. A CMOS transistor can be used as an access device to read and write (through the STT mechanism) a memory cell (STT-MRAM cell). The simulated read and write operations and related voltages are shown in Fig. 8. The ACM model accurately predicts the write delay and voltage levels, as well as the voltage oscillations during the signal transition. The MFF, introduced in [29], reduces the standby power of the flip-flops. As shown in Fig. 9, an MFF includes two MTJs that store a bit and complement of information. The information can, therefore, be retained after power is removed. The simulated

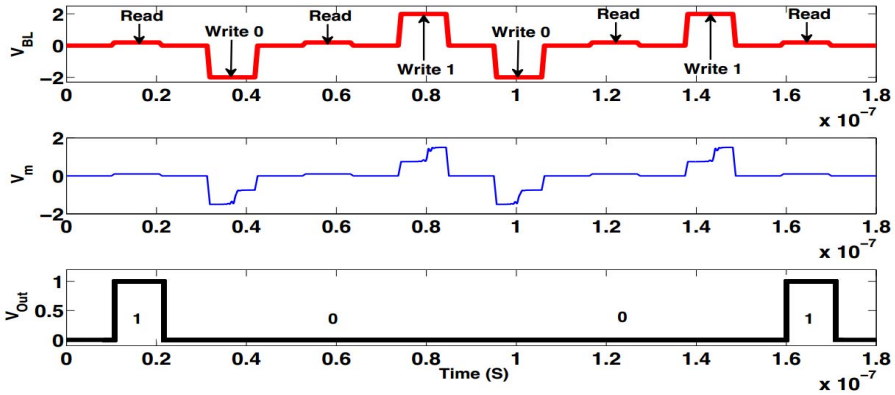


Fig. 8. Sequence of read/write operations of STT-MRAM. Switching delay, voltages, and transient oscillations are accurately predicted by the ACM model.

TABLE II
COMPARISON AMONG MTJ COMPACT MODELS

| Model | Asymmetric MTJ | Symmetric MTJ | Thermal Variations | Self-heating | Polarizing Layer | STT | VCMA |
|---|---|---|---|---|---|---|---|
| Zhao et al [11] | NO | YES | NO | NO | NO | YES | NO |
| Guo et al [14] | NO | YES | NO | YES | NO | YES | NO |
| Nigam et al [13] | NO | YES | NO | NO | NO | YES | NO |
| Harms et al [12] | NO | YES | NO | NO | NO | YES | NO |
| Panagopoulos et al [15] | NO | YES | YES | YES | NO | YES | NO |
| Kammerer et al [16], [17] | NO | YES | NO | NO | NO | YES | NO |
| Lee et al [18] | NO | YES | NO | YES | NO | YES | NO |
| Zhang et al [19] | NO | YES | YES | NO | NO | YES | NO |
| ACM model | YES | YES | YES | YES | YES | YES | YES |

TABLE III
COMPARISON AMONG ELECTRICAL MECHANISMS OF SWITCHING THE MAGNETIC STATE OF AN MTJ

| Mechanism | Power Consumption | Switching Time | Switching Type | Reliability |
|---|---|---|---|---|
| STT | High | Several nanosecond | Non-coherent | High, conditioned on sufficiently strong injected current |
| VCMA | Very low | Sub-nanosecond | Coherent | High, conditioned on tight control of applied pulse duration |
| STT-VCMA | Low | Few nanosecond | Non-coherent | High |

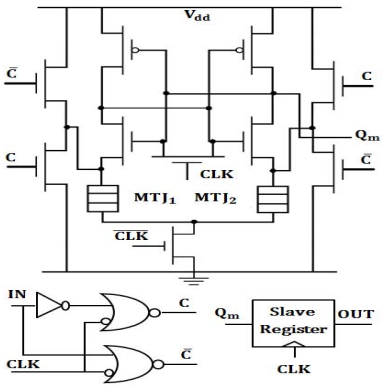


Fig. 9. Master–slave MFF.

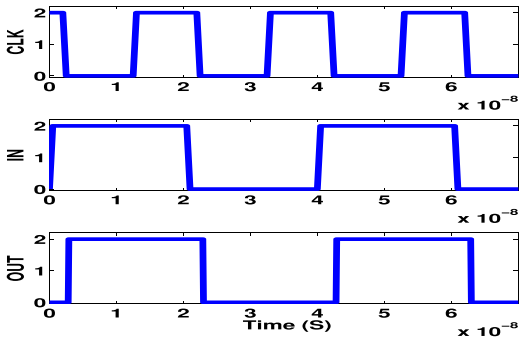


Fig. 10. Simulation of transient operation of the master–slave MFF. The ACM model is used for the MTJs and 45-nm PTM is used for the transistors.

operation of an MFF using the ACM model for the MTJs and a predictive transistor model (45-nm PTM) for the CMOS transistors is shown in Fig. 10. The pair of MTJs stores the data bit and complement.

## IV. COMPARISON OF MODELS

A comparison among different compact MTJ models is listed in Table II, and a comparison among the controlling mechanisms of the magnetic state of an MTJ is listed in Table III. In comparison with existing compact models, the ACM model includes the effects of asymmetry on the device behavior. The ACM model is therefore able to simulate both symmetric and asymmetric MTJs. Furthermore, the ACM model is the first compact model that considers the VCMA effect in MTJs. Accordingly, the ACM model is applicable to not only the STT-induced switching mechanism but also the VCMA-induced mechanism as well as any hybrid

method exploiting both the STT and VCMA effects. If an additional perpendicular polarizing layer is incorporated into the MTJ structure, the ACM model considers the effects of that layer on the device behavior. The ACM model can, therefore, be used to evaluate OST-MTJs [10], which exploits the perpendicular-to-the-plane polarizing layer.

The ACM model reduces to the compact models in [14], [15], and [18] if the asymmetry, VCMA, and polarizing layer effects are ignored. Furthermore, if the temperature and self-heating effects as well as the asymmetry, VCMA, and polarizing layer effects are ignored, the ACM model reduces to the compact models published in [16] and [17]. Note that the compact models in [11]–[13] consider a subclass of symmetric MTJs in which the VCMA is negligible, and only provide steady state results on the STT-induced switching mechanism. Furthermore, the compact models in [11]–[13] do not consider polarizing layer effects, and temperature and thermal variation effects. The compact model in [19] considers a subclass of symmetric PMTJs in which the VCMA is negligible, and produces the steady-state response to the STT-induced switching mechanism. The model in [19] does not consider self-heating effects. In fact, the models in [11]–[13] and [19] are not based on the LLG equation, so these models do not capture the transient behavior of the junction.

## V. Conclusions

A new compact model for MTJs, ACM model, is presented. The ACM model is a flexible compact model that characterizes an MTJ incorporating a free layer, an analysis layer, and a polarizing layer. The ACM model is validated using published experimental data. This model, developed under the single domain approximation, is computationally efficient. Furthermore, the ACM model considers both the STT and VCMA effects, and provides accurate results for any electrical controlling mechanism of magnetization switching in MTJs. The ACM model recognizes the effects of asymmetry on the physical behavior of the device, and is applicable to both symmetric and asymmetric MTJs. The ACM model also includes the dynamics of the junction temperature, permitting the effects of the system temperature on the device behavior to be considered.

## References


[1] M. Jullière, "Tunneling between ferromagnetic films," *Phys. Lett. A*, vol. 54, no. 3, pp. 225–226, Sep. 1975.

[2] E. Chen *et al.*, "Advances and future prospects of spin-transfer torque random access memory," *IEEE Trans. Magn.*, vol. 46, no. 6, pp. 1873–1878, Jun. 2010.

[3] W.-G. Wang, M. Li, S. Hageman, and C. L. Chien, "Electric-field-assisted switching in magnetic tunnel junctions," *Nature Mater.*, vol. 11, pp. 64–68, Nov. 2011.

[4] S. Kanai *et al.*, "Magnetization switching in a CoFeB/MgO magnetic tunnel junction by combining spin-transfer torque and electric field-effect," *Appl. Phys. Lett.*, vol. 104, no. 21, pp. 212406-1–212406-3, May 2014.

[5] J. Stöhr, H. C. Siegmann, A. Kashuba, and S. J. Gamble, "Magnetization switching without charge or spin currents," *Appl. Phys. Lett.*, vol. 94, no. 7, pp. 072504-1–072504-3, Feb. 2009.

[6] X. Yao, J. Harms, A. Lyle, F. Ebrahimi, Y. Zhang, and J. P. Wang, "Magnetic tunnel junction-based spintronic logic units operated by spin transfer torque," *IEEE Trans. Nanotechnol.*, vol. 11, no. 1, pp. 120–126, Jan. 2012.

[7] Z. Zeng *et al.*, "Ultralow-current-density and bias-field-free spin-transfer nano-oscillator," *Nature Sci. Rep.*, vol. 3, Mar. 2013, Art. ID 1426.

[8] D. C. Ralph, and M. D. Stiles, "Spin transfer torques," *J. Magn. Magn. Mater.*, vol. 320, no. 7, pp. 1190–1216, Dec. 2007.

[9] Y. Shiota, T. Nozaki, F. Bonell, S. Murakami, T. Shinjo, and Y. Suzuki, "Induction of coherent magnetization switching in a few atomic layers of FeCo using voltage pulses," *Nature Mater.*, vol. 11, no. 1, pp. 39–43, Nov. 2011.

[10] H. Liu, D. Bedau, D. Backes, J. A. Katine, J. Langer, and A. D. Kent, "Ultrafast switching in magnetic tunnel junction based orthogonal spin transfer devices," *Appl. Phys. Lett.*, vol. 97, no. 24, pp. 242510-1–242510-3, Dec. 2010.

[11] W. Zhao *et al.*, "Macro-model of spin-transfer torque based magnetic tunnel junction device for hybrid magnetic-CMOS design," in *Proc. IEEE Int. Workshop Behavioral Modeling Simulation*, Sep. 2006, pp. 40–43.

[12] J. D. Harms, F. Ebrahimi, Y. Xiaofeng, and W. Jian-Ping, "SPICE macromodel of spin-torque-transfer-operated magnetic tunnel junctions," *IEEE Trans. Electron Devices*, vol. 57, no. 6, pp. 1425–1430, Jun. 2010.

[13] A. Nigam, K. Munira, A. Ghosh, S. Wolf, E. Chen, and M. R. Stan, "Self consistent parameterized physical MTJ compact model for STT-RAM," in *Proc. IEEE Int. Symp. Semiconductors*, Oct. 2010, pp. 423–426.

[14] W. Guo *et al.*, "SPICE modelling of magnetic tunnel junctions written by spin-transfer torque," *J. Phys. D, Appl. Phys.*, vol. 43, no. 21, pp. 215001-1–215001-8, Jun. 2010.

[15] G. D. Panagopoulos, C. Augustine, and K. Roy, "Physics-based SPICE-compatible compact model for simulating hybrid MTJ/CMOS circuits," *IEEE Trans. Electron Devices*, vol. 60, no. 9, pp. 2808–2814, Sep. 2013.

[16] J. B. Kammerer, M. Madec, and L. Hèbrard, "Compact modeling of a magnetic tunnel junction—Part I: Dynamic magnetization model," *IEEE Trans. Electron Devices*, vol. 57, no. 6, pp. 1408–1415, Jun. 2010.

[17] J. B. Kammerer, M. Madec, and L. Hèbrard, "Compact modeling of a magnetic tunnel junction—Part II: Tunneling current model," *IEEE Trans. Electron Devices*, vol. 57, no. 6, pp. 1416–1424, Jun. 2010.

[18] S. Lee, H. Lee, S. Kim, S. Lee, and H. Shin, "A novel macro-model for spin-transfer-torque based magnetic-tunnel-junction elements," *Solid-State Electron.*, vol. 54, no. 4, pp. 497–503, Apr. 2010.

[19] Y. Zhang *et al.*, "Compact modeling of perpendicular-anisotropy CoFeB/MgO magnetic tunnel junctions," *IEEE Trans. Electron Devices*, vol. 59, no. 3, pp. 819–826, Mar. 2012.

[20] S. C. Oh *et al.*, "Bias-voltage dependence of perpendicular spin-transfer torque in asymmetric MgO-based magnetic tunnel junctions," *Nature Phys.*, vol. 5, pp. 898–902, Oct. 2009.

[21] J. C. Sankey *et al.*, "Measurement of the spin-transfer-torque vector in magnetic tunnel junctions," *Nature Phys.*, vol. 4, pp. 67–71, Nov. 2007.

[22] I. Theodonis, N. Kioussis, A. Kalitsov, M. Chshiev, and W. H. Butler, "Anomalous bias dependence of spin torque in magnetic tunnel junctions," *Phys. Rev. Lett.*, vol. 97, no. 23, pp. 237205-1–237205-6, Dec. 2006.

[23] J. Stöhr and H. C. Siegmann, *Magnetism: From Fundamentals to Nanoscale Dynamics* (Solid-State Sciences). New York, NY, USA: Springer-Verlag, 2006.

[24] J. C. Slonczewski, "Conductance and exchange coupling of two ferromagnets separated by a tunneling barrier," *Phys. Rev. B, Condens. Matter*, vol. 39, no. 10, pp. 6995–7002, Apr. 1989.

[25] W. F. Brinkman, R. C. Dynes, and J. M. Rowell, "Tunneling conductance of asymmetrical barriers," *Appl. Phys. Lett.*, vol. 41, no. 5, pp. 1915–1921, Jan. 1970.

[26] R. Stratton, "The influence of interelectronic collisions on conduction and breakdown in polar crystals," *Proc. Roy. Soc. A, Math., Phys. Eng. Sci.*, vol. 246, no. 1246, pp. 406–422, Aug. 1958.

[27] E. Salman and E. G. Friedman, *High Performance Integrated Circuit Design*. New York, NY, USA: McGraw-Hill, 2012.

[28] D. Fitzpatrick and I. Miller, *Analog Behavioral Modeling With the Verilog—A Language*. New York, NY, USA: Springer-Verlag, 1998.

[29] W. S. Zhao, E. Belhaire, and C. Chappert, "Spin-MTJ based non-volatile flip-flop," in *Proc. IEEE Conf. Nanotechnol.*, Aug. 2007, pp. 399–402.

**Mohammad Kazemi** (S'10) received the M.Sc. degree in communication systems from K.N.Toosi University of Technology, Iran in 2010 and the M.Sc. degree in electrical and computer engineering from the University of Rochester, USA in 2014. His primary research interests include emerging memory technologies, information theory, and the convergence of microelectronic circuits with information theory.

**Engin Ipek** (M'09) is assistant professor of ECE and CS at the University of Rochester. He received his Ph.D. in ECE from Cornell University in 2008. He is a recipient of the 2014 IEEE Computer Society TCCA Young Computer Architect Award, two IEEE Micro Top Picks awards, an ASPLOS 2010 best paper award, and an NSF CAREER award.

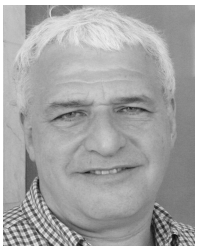

**Eby G. Friedman** (F'00) is a Distinguished Professor with the University of Rochester, Rochester, NY, USA and a Visiting Professor with the Technion-Israel Institute of Technology. He is the author of almost 500 papers, book chapters, patents, and books in the fields of high speed and low power CMOS circuits, 3-D integration, and synchronous clock and power delivery. Dr. Friedman is a senior Fulbright Fellow.